Preparation of Multicore Colloidosomes: Nanoparticle-Assembled Capsules with Adjustable Size, Internal Structure, and Functionalities for Oil Encapsulation

*David F.F. Brossault [1,2], Thomas M. McCoy [1,2] and Alexander F. Routh [1,2]**

1. *Department of Chemical Engineering and Biotechnology, University of Cambridge, Philippa Fawcett Dr, Cambridge CB3 0AS, United Kingdom*
2. *BP Institute, University of Cambridge, Madingley Rise, Cambridge CB3 0EZ, United Kingdom*

E-mail: afr10@cam.ac.uk

Abstract

Colloidosomes, also known as Pickering emulsion capsules, have attracted considerable attention for encapsulation of both hydrophilic and hydrophobic actives. However, current preparation methods are limited to single core structures and require modified/engineered nanoparticles for forming the capsules. Here, a simple, safe, and highly versatile approach for producing multicore colloidosomes from non-modified nanoparticles is reported. Multi-oil core silica colloidosomes are prepared at room temperature via salt-driven assembly of cheap hydrophilic nanoparticles dispersed within a double (O/W/O) emulsion template. The internal structure and overall diameter of the final capsules can be adjusted by altering the primary and secondary emulsification conditions. With this approach, 7 to 35 µm diameter capsules containing 0.9 to 4.2 µm diameter multiple oil cores are produced. Nanoparticles such as Fe_3O_4, TiO_2 and ZnO can easily be incorporated within the structure, conferring magnetic and photocatalytic properties to the capsules, enabling degradation of Rhodamine B under UV-light irradiation as well as magnetic capture. These capsules can also be used to entrain hydrophobic dye (Nile red), with ultrasound rupturing serving as a facile method for accessing the internal core environments. This work offers a promising approach for producing tunable multifunctional microcapsules for oil encapsulation.

Keywords: Multicore colloidosome, Double emulsion, Nanoparticle, Self-assembly, Magnetism, Photocatalysis, Oil encapsulation.

1. Introduction

Microencapsulation has attracted much research interest for protecting and delivering active ingredients in food and beverage,[1,2] cosmetic and personal care,[3,4] agrochemical [5,6] and pharmaceutical [7,8] applications. The method consists of the entrainment of a solid, liquid, or gaseous compound, called the active material, within another structure referred to as the shell. This approach offers multiple advantages.[9] Firstly, the shell acts as a protective layer providing greater stability of the active material when exposed to adverse environmental conditions (i.e. light irradiation, humidity, temperature, pH). The shell can also act as a layer for protecting the surrounding environment from the toxicity of the active ingredient, as in the case of potent pharmaceutical drugs. Secondly, the use of a core/shell system provides better control of the delivery of the encapsulated material. Depending on the shell composition, thickness and permeability, active ingredients can be released over longer time ranges or upon application of chemical (e.g. addition of acid) or mechanical (e.g. ultrasound) triggers. Finally, microencapsulation can also provide practical advantages, by masking the taste or odor of an active or improving its handling.

Multiple encapsulation techniques have been reported using thermal, electrostatic, or chemical methods to produce core/shell capsules.[9,10] Among them, colloidosomes appear as a promising system. Such capsules, originally reported by Velev and co-workers [11] and named by Dinsmore et al. [12], are composed of a gel or liquid core surrounded by a nanoparticle-assembled shell. [13,14] These superstructures offer high control on permeability,[15,16] functionalities [17-19] and release mechanisms, [20-24] depending on the preparation method and choice of shell colloidal particles. Colloidosomes are conventionally produced via a two-step approach. First, a particle stabilized or *Pickering* emulsion, [25] is formed via adsorption of colloidal particles at an oil/water interface. Particles must exhibit affinity for both the aqueous and organic phases, which often requires adjustment of particle wettability by the adsorption of additives (e.g. surfactants, polymers) or chemical functionalization. [26,27] Particles are then locked at the interface, producing a robust microcapsule for utilization. [13,14]

Depending on the preparation method, colloidosomes can be used for encapsulation of hydrophilic or hydrophobic actives. Active materials such as yeasts, [28] bacteria, [29] enzymes, [30] or therapeutic molecules [31] have been successfully encapsulated within water-core colloidosomes. Many authors have reported oil-core colloidosomes, aiming to address the usual volatility or stability concerns inherent with hydrophobic actives (e.g. Flavors, fragrances,

antioxidants, vitamins, pesticides, etc.). [32-44] These oil-core systems are conventionally produced from a Pickering-emulsion template, with particles locked together in a robust shell through thermal annealing, [16] layer-by-layer polyelectrolyte deposition, [33-35] ionotropic gelation, [36,37] cross-linking, [38-40] interfacial polymerization [41] or growing of an additional inorganic [42, 43] or metallic shell [44]. However, such approaches exhibit certain limitations. Firstly, the need for an intermediate Pickering emulsion step, requires the design/modification of nanoparticles to obtain suitable Pickering emulsifiers, raising the cost and complexity of the method. Secondly, the locking step may be time-consuming and costly due to modification of experimental conditions (e.g. pH, Temperature) or further addition of toxic chemicals to the system (i.e. Cross-linkers, polymers, polyelectrolytes), which may impact the stability of encapsulated actives. Finally, only single core systems have been reported, limiting the potential of these structures because of the single-step release mechanism. Producing multicore colloidosomes could enable encapsulation of multiple hydrophobic cargoes, enabling a multi-stage release of actives. To the best of our knowledge, multicore colloidosomes have only been reported once. [45] In their work, Lee and Weitz described the preparation of non-spherical multi-compartment colloidosomes obtained from assembly of hydrophobic particles within a Water-in-Oil-in-Water (W/O/W) emulsion template. However, this approach was limited to a water-core structure and required the use of a solvent evaporation approach for producing the capsules.

Here, we present a facile, safe, and adjustable method for producing spherical multicore colloidosomes via salt-driven assembly of commercial nanoparticles in an Oil-in-Water-in-Oil (O/W/O) emulsion template. In this approach, capsules are prepared at room temperature without requiring an intermediate Pickering-emulsion template. The use of a colloidal destabilization approach as a locking mechanism makes this method environmentally benign. Furthermore, the internal structure and functionalities of the final capsules can be easily tuned by altering the mixing conditions and composition of the aqueous phase.

2. Results and discussion

Silica nanoparticles used in these experiments are strongly hydrophilic, inhibiting their adsorption at the oil/water interface for formation of Pickering emulsions. However, these particles can easily be destabilized, and aggregate upon addition of salt. When these particles were dispersed in ultrapure water, the pH increased slightly to values between 9 and 10. In this pH range, the silica nanoparticles readily disperse and bear a strong negative surface charge measured between -40 and -50 mV. Addition of calcium chloride induces surface charge screening and subsequent nanoparticle agglomeration. This hetero-coagulation approach has recently been reported in reverse emulsions for room-temperature production of magnetic silica microparticles (Fe_3O_4/SiO_2) [46] and magnetic photocatalysts ($TiO_2/Fe_3O_4/SiO_2$) [47]. Here, formation of an O/W/O emulsion serves to structurally template assembly of the capsules, with multiple oil cores embedded within their structure.

The major advantage of the present approach for capsule formation is that it circumvents the necessity for creation of a Pickering emulsion. This can be challenging to achieve, as the colloidal particles must have an inherent affinity for the oil-water interface. Such particles are often surface functionalised (ie. Janus particles) or incorporated with additives to facilitate interfacial adsorption (ie. Polymers or charged surfactants), making the system more complex and expensive. The current method allows for formation of capsules by aggregating purely hydrophilic commercial nanoparticles that are dispersed in the aqueous medium surrounding the surfactant stabilised oil droplets. Therefore, the nanoparticles can be used directly, without adjusting their wettability. The complete preparation method is displayed in **Scheme 1**.

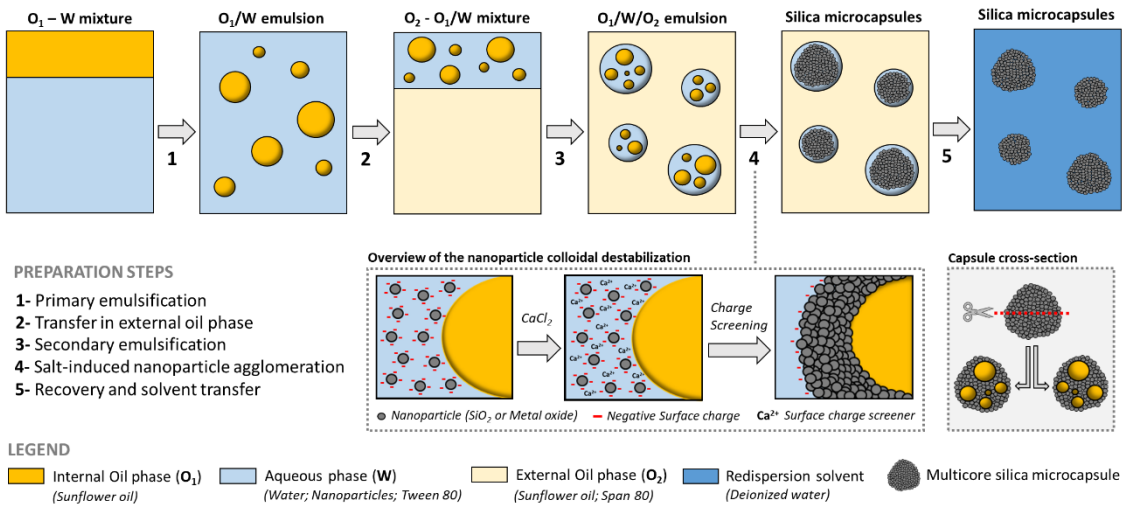

Scheme 1. General procedure for preparing multi-oil core silica microcapsules using commercial nanoparticles dispersed in an Oil-in-Water-in-Oil emulsion template.

2.1. Preparation of multicore capsules with tunable core size and overall diameter

In our preparation method, the capsule structure is directly controlled by utilisation of primary and secondary emulsions, with the former templating the inner cores and the latter templating the overall capsule size. Therefore, size and stability of these emulsions is crucial in the design of our capsules. Preliminary experiments were carried out to investigate the impact of mixing conditions and surfactant concentration on emulsion preparation (**Figures S1** to **S4**). Results showed that primary (O_1/W) emulsions prepared with 5 wt% Tween 80 were stable for more than 24 h and the diameter of the dispersed droplets could easily be adjusted between 0.9 and 4.2 µm, depending on the mixing conditions. Double (O_1/W/O_2) emulsions, prepared from those primary emulsions, were stable for 30 min, enabling their use as microcapsule template.

The impact of primary emulsification parameters on the capsule internal structure was first assessed by producing capsules from double emulsions prepared at different primary emulsification conditions (Ultra-Turrax (UT) operating at 5,000, 10,000 or 15,000 RPM), and fixed secondary emulsification conditions (Vortex mixer (V) operating at 2,000 RPM). Microscopy images confirmed the production of spherical capsules with an average overall diameter of approximately 18 µm, regardless of mixing parameters (**Figure 1**). STEM and optical microscopy images confirmed the presence of multiple cores within the capsules, and showed a significant decrease in internal core diameter with increased mixing speeds (3.3 to 0.8 µm). The size of these cores correlates with the diameter of oil droplets dispersed in the primary emulsions (**Figure S1**), confirming that primary emulsification conditions dictate the capsule internal structure. By increasing the energy input, primary emulsions with smaller oil droplets are formed and subsequently used to template smaller oil cores within the final capsule structure. Triplicated samples confirmed the repeatability of the procedure, with deviation in overall capsule and inner core diameters being less than 15%. Optical microscopy images, average core size and overall capsule diameter values of those samples are provided in the Supporting Information (**Figure S5**).

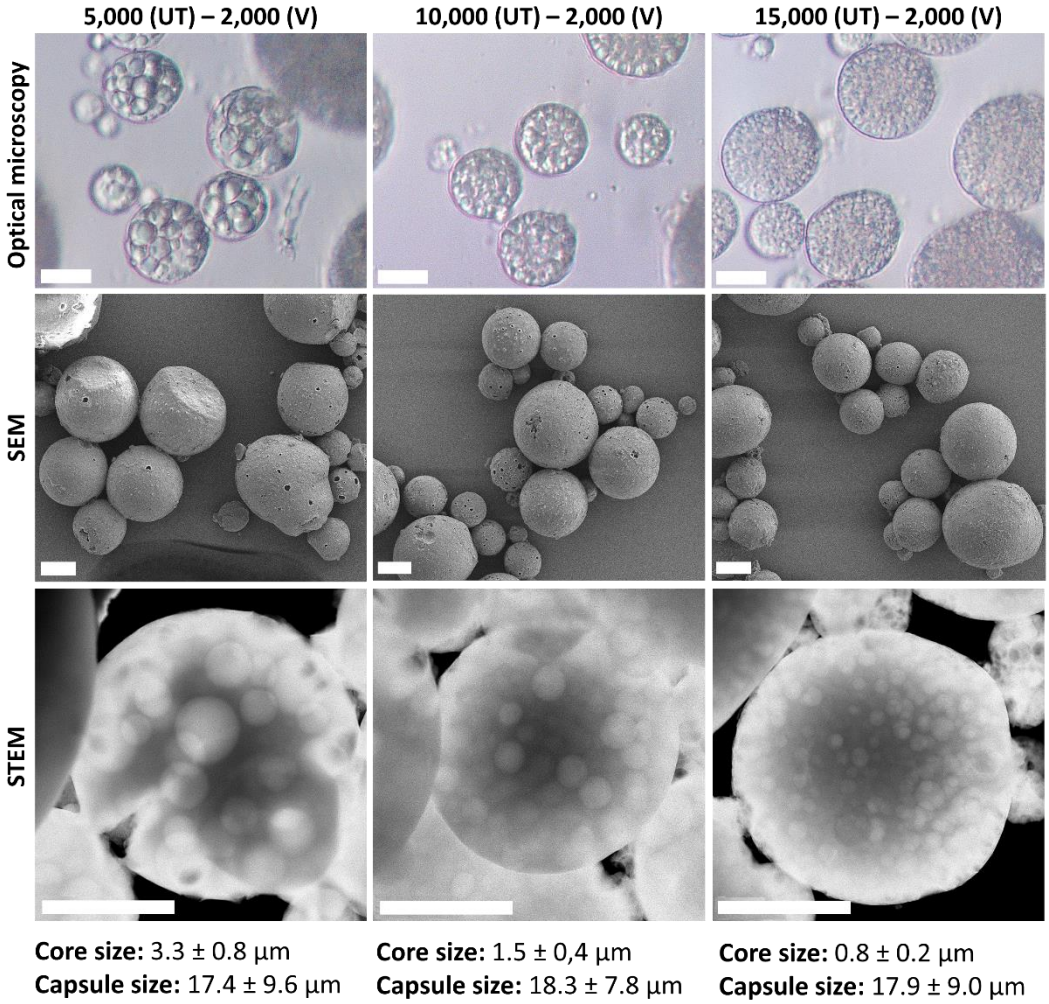

Figure 1. Microscopy images of multi-oil-core silica microcapsules prepared with different primary emulsification mixing speeds (shown at the top of the figure). Scale bars are equal to 10 µm. Average size values were obtained from the analysis of optical microscopy images (N=250).

The surface defects, observed by SEM (**Figure 1**), are likely to be due to the presence of oil cores adjacent to the double emulsion boundaries prior to capsule formation. In this instance, incomplete trapping of the core, within the capsule, results in a shell defect whereby the core is already exposed via a hole or space in the capsule surface. Additional SEM images suggest that the size and frequency of such defects can be significantly reduced by decreasing the diameter of the internal oil cores. This helps to ensure that they are more likely to locate completely within the capsule confines. An alternative solution could be to reduce the overall ratio of oil within the capsules, enabling enhanced diffusion of oil droplets within double emulsions prior to colloidal destabilization.

The impact of secondary emulsification parameters on overall capsule structure was investigated, by producing capsules from double emulsions prepared at different primary (UT operating at 5,000, 10,000 or 15,000 RPM) and secondary (Manual mixing, V or UT operating at diverse speeds) emulsification conditions (**Figure 2**). A decrease in the overall capsule diameter was observed for samples prepared using the higher energy input technique (UT), and this was found to occur irrespective of primary emulsification conditions (**Figure 2A-C**). By increasing the energy input during the secondary emulsification step, smaller double emulsions are produced resulting in smaller capsules. Using this approach, multicore silica capsules with an overall diameter between 7 and 35 µm can be produced.

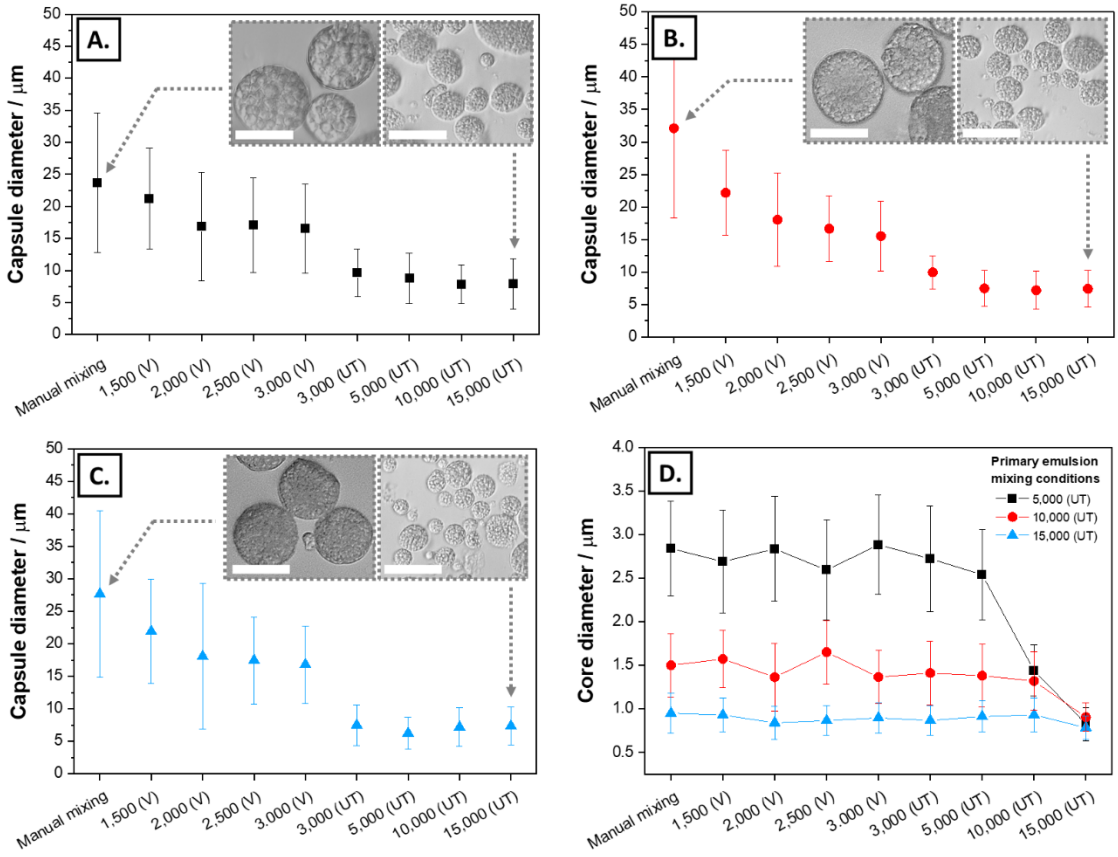

Figure 2. Impact of secondary emulsification mixing speed on **(A-C)** overall capsule diameter and **(D)** inner core diameter. Capsules obtained using primary emulsions prepared with an Ultra-Turrax operating at **(A)** 5,000, **(B)** 10,000 and **(C)** 15,000 RPM. Insets are optical microscopy images of capsules produced at the indicated mixing conditions. Scale bars are equal to 20 µm.

Measurement of internal core diameters showed that secondary emulsification conditions can also impact the capsule internal structure when increased to some extremes, as evidenced by the decrease in core diameter measured for capsules prepared from a larger primary emulsion

at high mixing speed (10,000 or 15,000 (UT)) (**Figure 2D**). At this secondary mixing speed, oil droplets are further dispersed within the double emulsion, resulting in a reduction of average core diameter from 2.8 to 0.8 µm. Therefore, a reduced mixing speed should be exploited to produce small capsules with large oil cores. Optical microscopy images of all samples are provided in the Supporting Information (**Figure S6**).

These results show that capsules produced using this method possess a high degree of tunability, enabling tailoring of their internal structure and overall size by simply adjusting the mixing conditions.

2.2. Facile shell functionnalization

Metal doped multicore colloidosomes were prepared via dispersion of Fe_3O_4, TiO_2 or ZnO nanoparticles within the aqueous phase prior to capsule formation. EDS elemental mapping analysis confirmed the successful incorporation of nanoparticles within the capsule structure (**Figure 3A-C**). Optical microscopy images and size distribution histograms showed that this incorporation did not alter the size or structure of the final capsules, resulting in 17 to 20 µm large capsules with 1 µm cores .

The incorporation of various nanoparticles within the capsule structure confers additional physicochemical properties to the system. For instance, exposing Fe_3O_4-doped microcapsules to an external magnetic field resulted in their recovery from solution in fewer than 30 seconds (**Figure 3D**). Photocatalytic properties of TiO_2 and ZnO doped capsules were investigated by exploring the degradation of a synthetic dye (Rhodamine B) upon UV-light irradiation. Results display enhanced dye removal for capsules integrating these metals (**Figure 3E**). In the absence of capsules, minimal degradation of Rhodamine B under UV-light irradiation was observed, confirming the dye stability and importance of the photocatalytic materials. In the presence of multicore silica colloidosomes without metal dopants, a 16% decrease in dye absorbance was observed after 1 hour of UV irradiation. Beyond 10 minutes, any additional irradiation does not result in further decreases in absorption, suggesting that the mechanism may be due to adsorption from solution rather than photodegradation. The capsules bear a negative surface charge at neutral pH, and since Rhodamine B features a cationic quaternary ammonium group, this mechanism is feasible. The observed plateau is due to saturation of the capsule surfaces with Rhodamine B, preventing further removal from solution.

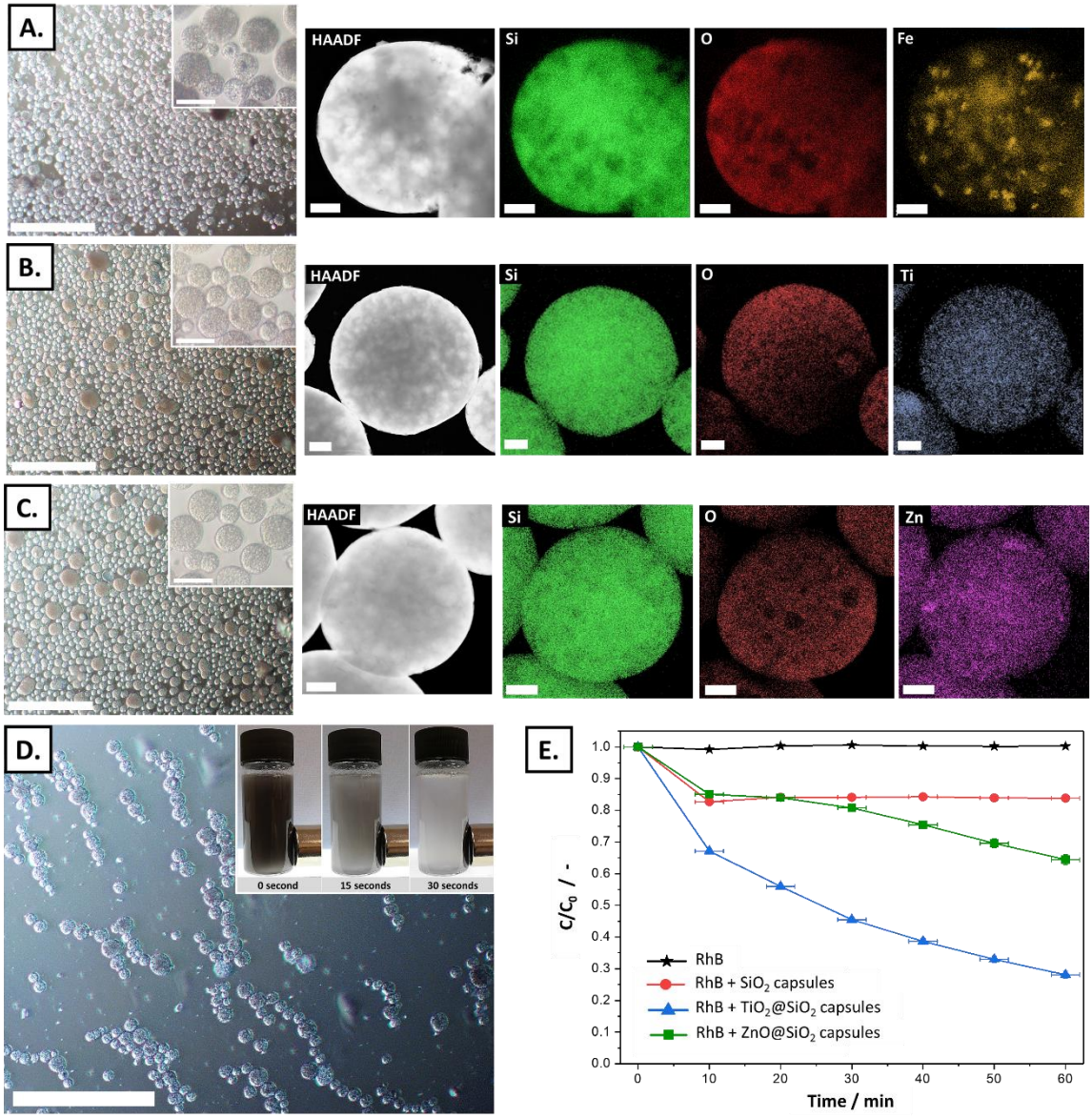

Figure 3. Doping of multicore silica microcapsules (15,000 (UT) – 2,000 (V)) with Fe_3O_4, TiO_2 or ZnO nanoparticles. Optical microscopy images and EDS elemental mapping of capsules doped with **(A)** Fe_3O_4, **(B)** TiO_2 and **(C)** ZnO nanoparticles. (**D**) Response of Fe_3O_4 doped capsules to external magnetic fields. **(E)** Degradation of a Rhodamine B solution (50 mL, 10 $mg.L^{-1}$) under UV-light irradiation in the presence of TiO_2 and ZnO doped capsules (100 mg). Dye degradation experiments have been duplicated, the Y-axis standard deviations were measured below 3% and therefore not plotted on this graph. Scale bars are equal to 200 µm on optical microscopy images (20 µm on inset images) and to 2 µm on STEM images.

In the presence of TiO_2 doped capsules, a 72% decrease in the absorption maxima were observed after 1 h of UV irradiation. The corresponding result for ZnO doped capsules was 36%. The steady decrease observed over time confirms that photodegradation is the key mechanism impacting changes in absorption properties. Absorbance spectra in these cases exhibit both a decrease in the maximum absorbance as well as a hypsochromic shift (towards

lower wavelengths), characteristic of degradation of an aromatic ring and de-ethylation of Rhodamine B [48-50]. The difference in degradation efficiency between the two systems is likely to arise from the lower amount of metal dopant within the ZnO capsules compared to those with TiO_2. Adjusting the loading of nanoparticles within the capsules as well as capsule diameter or light source conditions, would likely alter the degradation dynamics. Additional EDS mapping analysis, optical microscopy images, size distribution histograms and absorbance spectra are provided in the Supporting Information (**Figures S7** to **S9**).

This approach enables facile, fast, and diverse capsule production and functionalization, without the need for nanoparticle surface modification or post-production capsule coating. This work has demonstrated the incorporation of Fe_3O_4, TiO_2 and ZnO nanoparticles, although other materials (e.g. metal oxides, charged polymeric particles, carbon nanodots) could be included within the capsule structure, provided they can be homogeneously dispersed in the aqueous phase and destabilized upon addition of salt.

2.3. Rupture of capsules with ultrasound

Ultrasound was applied to multicore silica microcapsules to assess their structural integrity (**Figure 4A**). Microscopy performed before and after treatment provided key structural information (**Figure 4B-E**). The presence of oil cores within the capsules was easily confirmed by the difference in contrast observed between the embedded oil droplets and silica shell. After applying ultrasound, non-miscible droplets and shell fragments were observed in solution confirming capsule rupture and release of the hydrophobic contents (i.e. sunflower oil). Images obtained after increased ultrasound duration suggest a direct correlation between the capsule internal structure and robustness. Capsules with large cores were observed to break into non-spherical fragments upon ultrasonication, resulting in complete rupture of the capsules after 3 min of treatment (**Figure 4B** and **4D**). Fragments observed following rupture did not show any apparent contrast within their structure, suggesting complete release of sunflower oil. Conversely, capsules with smaller cores remained spherical upon ultrasonication (**Figure 4C** and **4E**). Increasing the ultrasound duration appeared to result in superficial erosion with spherical capsules 17, 38 and 50% smaller after 1, 2, and 3 min of ultrasound. The contrast observed within the final capsules suggests the presence of residual oil cores, still available for further release steps. This ability to adjust the capsule robustness by simple modification of the internal structure makes the method promising for producing versatile capsules for use in triggered release applications.

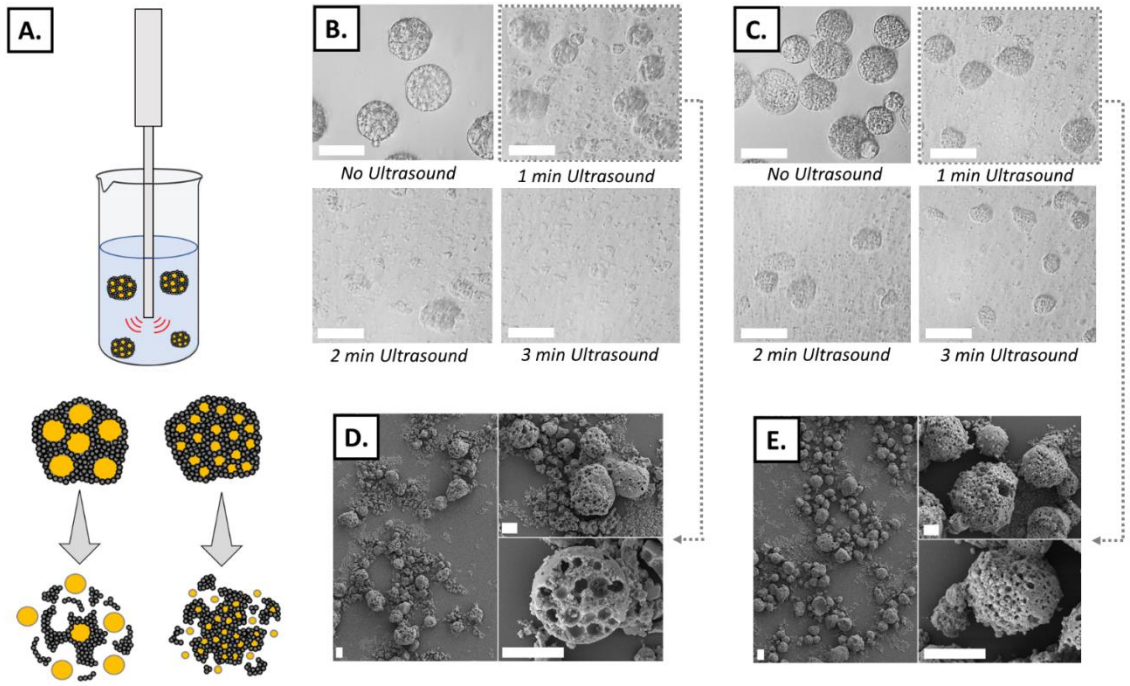

Figure 4. Rupture of capsules using ultrasound. **(A)** Schematic of the sonication and rupturing process. Optical microscopy images of **(B)** 5,000 (UT) - 2,000 (V) and **(C)** 15,000 (UT) – 2,000 (V) capsules after 0 min, 1 min, 2 min or 3 min of ultrasound. Scanning electron microscopy images of **(D)** 5,000 (UT) - 2,000 (V) and **(E)** 15,000 (UT) – 2,000 (V) capsules after 1 min of ultrasound. Scale bars are equal to 20 µm.

Observation of broken capsules via SEM confirmed the multicore structure with average inner core diameters of 2.8 ± 0.5 and 0.9 ± 0.2 µm for 5,000(UT)-2,000(V) and 15,000(UT)-2,000(V) capsules. Those values are in concurrence with the results obtained from optical microscopy and STEM images (**Figure 1**). Low magnification optical microscopy images of samples after ultrasound and additional SEM images of capsules after 1 min of ultrasound are provided in the Supporting information (**Figures S10** and **S11**).

2.4. Encapsulation of a hydrophobic compound

Nile red was used to confirm the capacity of the capsules to retain hydrophobic compounds within their structure. A pink solid was visually observed following capsule cleaning, suggesting encapsulation of dye within the structure. Confocal microscopy images of Nile red loaded capsules taken 48 h after preparation exhibited bright pink spots (**Figure 5**). This observation confirms encapsulation of hydrophobic dye, as well as a multi-oil core structure, corroborating the results from STEM, SEM and optical microscopy.

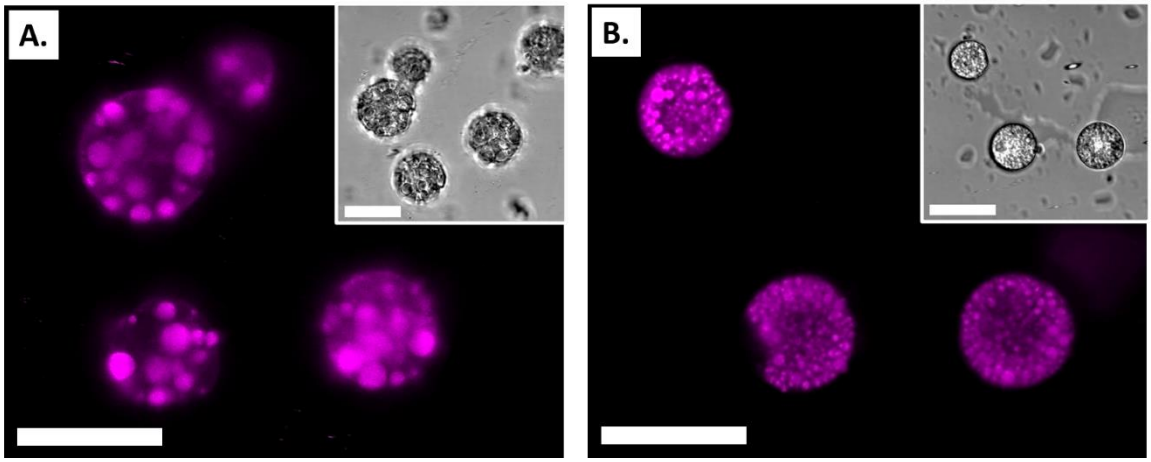

Figure 5. Confocal microscopy images of **(A)** 5,000 (UT)-2,000 (V) and **(B)** 15,000 (UT) – 2,000 (V) capsules loaded with Nile red. Insets are the corresponding bright field images. Scale bars are equal to 20 µm.

3. Conclusion

This paper reports a novel method for producing multi-oil core silica colloidosomes via salt-driven assembly of nanoparticles in an Oil-in-Water-in-Oil emulsion template. In this approach, capsules are produced without requiring a Pickering emulsion intermediate step, enabling direct use of nanoparticles without any surface functionalization or surfactant adsorption. This approach offers multiple advantages compared to conventional encapsulation techniques. Firstly, the capsules are easy to produce with minimal lab equipment, offering exceptional promise for scalability. Secondly, the entire process can be undertaken at room temperature without harmful or toxic reagents, making the synthesis and final product environmentally friendly. Finally, the emulsion templating route provides a high degree of versatility for controlling the physicochemical properties of the final material. We demonstrate incorporation of Fe_3O_4, TiO_2 and ZnO nanoparticles within the structure for specialised functionalities: magnetic removal and photocatalysis. It is also possible to control the overall size of the capsules as well as the inner core dimensions by adjusting mixing conditions and system composition. These capsules were able to retain a hydrophobic dye (Nile red) within their structure and could be ruptured by ultrasound, enabling direct access to the inner cores. We believe this work showcases an effective procedure for producing a novel multifunctional colloidal material that can be tailored for a variety of industrial applications using cheap, commercially available nanoparticles as building blocks.

4. Experimental section

Materials

All chemicals were obtained from Sigma-Aldrich or Fisher scientific, except where otherwise specified, and were used without further purification: Sunflower oil (Sainsburys), Absolute ethanol, Ludox HS-40 (SiO_2, 40 wt% in H_2O, 15-25 nm diameter), Tween 80, Span 80, Calcium chloride dihydrate ($CaCl_2$, $2H_2O$), Nile Red (Dry powder, 99%), Rhodamine B (Dry powder, 95%), Iron (II, III) oxide (Fe_3O_4, dry powder, 50 – 100 nm diameter), Titanium dioxide (TiO_2, dry powder, 21 nm diameter, 99.5%) and Zinc oxide (ZnO, 20 wt% in H2O, < 100 nm diameter). Note: Ludox HS40 was used 6-12 months after opening and exhibited a higher viscosity compared to freshly opened bottles. We believe this was likely due to progressive hydrolysis of the silica nanoparticle surface over time. Supplementary experiments confirmed that the same trends could be observed with fresh Ludox HS40 bottles. Adjusting the surfactant concentration serves to compensate for the difference in viscosity (**Figures S12** to **S15**).

Preparation of simple and double emulsions

Oil-in-Water (O_1/W) primary emulsions and Oil-in-Water-in-Oil (O_1/W/O_2) secondary emulsions were prepared for use as capsule templates. The aqueous phase (W) was prepared by addition of silica nanoparticles (35 wt%) and Tween 80 (1, 5 or 10 wt%) to deionized water. The internal oil phase (O_1) was composed of sunflower oil. External oil phase (O_2) was composed of sunflower oil and Span 80 (1 wt%). Primary emulsions were prepared by mixing the internal oil phase (2 g) with the aqueous phase (8 g) for 60 s using an Ultra Turrax mixer (T 25 digital, IKA) set at 3,000, 5,000, 10,000 or 15,000 RPM. Secondary emulsions were prepared by mixing the primary emulsion (1 g) and the external oil phase (9 g) for 60 s using a Vortex mixer (TopMix FB15024, Fischer Scientific) set at 2,000 RPM. The stability of different emulsions was assessed at regular time intervals using visual observation and optical microscopy.

Preparation of multi-oil core silica capsules

Oil core microcapsules were prepared from O_1/W/O_2 double emulsions using the method presented in Scheme 1. The concentration of Tween 80 in the aqueous phase was set to 5 wt% and secondary emulsification was carried out using either a Vortex (V) or an Ultra Turrax (UT) mixer. For metal oxide doping experiments, Fe_3O_4 (5 wt%), TiO_2 (5 wt%) or ZnO (1.5 wt%) nanoparticles were added to the aqueous phase before homogenization for 5 min (30 s on – 10 s off) with an ultrasonic homogenizer (Sonic Dismembrator FB-120, Fisher Scientific).

Capsules were then formed after dropwise addition of a calcium chloride solution (1 mL, 1 mol.L^{-1}) into the $O_1/W/O_2$ emulsion, whilst maintaining 2,000 RPM stirring with a Vortex mixer (V). The capsules were then recovered from solution via centrifugation (3,000 RPM, 5 min) and cleaned twice by sequential centrifugation (2,000 RPM, 5 min) and redispersal in deionized water.

Structural characterisation of emulsions and capsules

The internal structure, overall diameter and chemical composition of the capsules were assessed using optical and electron microscopy. Optical microscopy images were obtained using a Leica DME microscope equipped with 10× and 63× objective lenses. Scanning Electron Microscopy (SEM) images were taken using a Tescan Mira3 FEG-SEM microscope (acceleration voltage of 5 kV). Scanning transmission electron microscopy (STEM) images were obtained using a Talos F200X G2 from Thermo Scientific equipped with a Ceta 16 M camera at an acceleration voltage of 200 kV. The same setup was used to examine incorporation of metal oxides into the structure via Energy Dispersive X-ray spectroscopy (EDS). The diameters reported in this article were obtained using ImageJ software (imagej.net), analysing 250 randomly chosen droplets or capsules. All reported values include a confidence interval corresponding to one standard deviation.

Shell rupture and access to internal cores

Rupture of capsules was instigated using an ultrasonic homogenizer: 5 mL of solution containing multicore capsules were ultrasonicated for up to 3 min. Samples were then centrifuged (5,000 RPM – 5 min) and cleaned twice with absolute ethanol before being redispersed in 5 mL of deionized water and observed with optical and electron microscopy.

Magnetic properties of Fe_3O_4 doped capsules

The magnetic response of Fe_3O_4 doped silica microcapsules was assessed via exposure to an external magnetic field. For this, 12 mL of aqueous solution containing 20 mg.L^{-1} of Fe_3O_4 doped silica capsules was exposed to a magnetic field generated by a Rare-earth neodymium magnet (NiCuNi, 20x20 mm, E-magnets UK). Pictures were taken every 15 seconds to analyse the separation process.

Photocatalytic properties of TiO_2 and ZnO doped capsules

The photocatalytic properties of TiO_2 and ZnO doped silica microcapsules were assessed via degradation of Rhodamine B solution under UV-light irradiation. Sample preparation involved 100 mg of capsules being added to a Rhodamine B solution (50 mL, 10 $mg.L^{-1}$). The solutions were then exposed to UV-light (36 W, Light excitation: 365 nm). 5 mL of solution was collected after 0, 10, 20, 30, 40, 50 and 60 minutes and centrifuged at 5,000 RPM for 5 min. Absorbance of the supernatant was measured using a UV-visible spectrophotometer (Cary 60, Agilent technologies). The absorption maximum was observed to shift from 555 to 528 nm, and therefore was not interpreted at a fixed wavelength but at the position of the maximum. The compacted capsules were then redispersed by manual agitation with the supernatant, and the mixture was reinjected into the original solution. This procedure was repeated at subsequent time intervals. Rhodamine B solution with and without SiO_2 microcapsules were used as references. Each experimental series was duplicated to ensure reproducibility of results.

Preparation and characterization of Nile red loaded capsules

Capsules containing Nile red (150 $mg.L^{-1}$) were prepared. Initially, primary emulsions were prepared using an Ultra-Turrax mixer operating at 5,000 or 15,000 RPM and secondary emulsions were prepared using a Vortex mixer operating at 2,000 RPM. The formed capsules were imaged using a Leica SP5 confocal microscope equipped with a 63x oil objective (Excitation wavelength: 514 nm, Detector range: 530-730 nm).

Conflict of Interest

The authors declare no conflict of interest.

Acknowledgements

The authors gratefully acknowledge Dr Heather Greer and Luca Mascheroni from the Department of Chemistry and the Department of Chemical Engineering and Biotechnology at the University of Cambridge for their help with STEM, EDS analysis and confocal microscopy experiments. The authors also thank Dan Toy and Eleftheria Diamanti, for their help with some of the initial experiments. The authors acknowledge the EPSRC Underpinning Multi-User Equipment Call (EP/P030467/1) for funding the Talos, used for STEM and EDS analysis. D.F.F.B. thanks the University of Cambridge for funding through a W.D. Armstrong PhD Scholarship. T.M.M. thanks the Ernest Oppenheimer Fund for funding through an Oppenheimer Research Fellowship.

References

[1] B.F. Gibbs, S. Kermasha, I. Alli, C.N. Mulligan, *Int. J. Food Sci. Nutr.* **1999**, 50, 213.

[2] S. Gouin, *Trends Food Sci. Technol.* **2004**, 15, 330.

[3] I.T Carvalho, B.N Estevinho, L. Santos, *Int. J. Cosmet. Sci.* **2016**, 38, 109.

[4] F. Casanova, L. Santos, *J. Microencapsul.* **2016**, 33, 1.

[5] B. Hack, H. Egger, J. Uhlemann, M. Henriet, W. Wirth, A.W.P. Vermeer, D.G. Duff, *Chem. Ing. Tech.* **2012**, 84, 223.

[6] K. Tsuji, *J. Microencapsul.* **2001**, 18, 137.

[7] M.N. Singh, K.S.Y. Hemant, M. Ram, H.G. Shivakumar, *Res Pharm Sci.* **2010**, 5, 65.

[8] G. Ma, *J. Control Release* **2014**, 193, 324.

[9] H.N. Yow, A.F. Routh, *Soft Matter* **2006**, 2, 940.

[10] R. Dubey, T.C. Shami, K.U.B. Rao, *Def. Sci. J.* **2009**, 59, 82.

[11] O.D. Velev, K. Furusawa, K. Nagayama, *Langmuir* **1996**, 12, 2374.

[12] A.D. Dinsmore, M.F. Hsu, M.G. Nikolaides, M. Marquez, A.R. Bausch, D.A Weitz, *Science* **2002**, 298, 1006.

[13] F.J. Rossier-Miranda, C.G.P.H. Schroën, R.M. Boom, *Colloids and Surfaces A: Physicochem. Eng. Aspect* **2009**, 343, 43.

[14] K.L Thompson, M. Williams, S.P. Armes, *J. Colloid. Interf. Sci.* **2015**, 447, 217.

[15] J.W. Kim, A. Fernandez-Nieves, N. Dan, A. S. U, M. Marquez, D. A. Weitz, *Nano Lett.* **2007**, 7, 2876.

[16] H.N. Yow, A.F. Routh, *Langmuir* **2009**, 25, 159.

[17] H. Duan, D. Wang, N.S. Sobal, M. Giersig, D.G. Kurth, H. Mohwald, *Nano Lett.* **2005**, 5, 949.

[18] L. Zhang, F. Zhang, Y.S. Wang, Y.L. Sun, W.F. Dong, J.F. Song, Q.S. Huo, H.B. Sun, *Soft Matter* **2011**, 7, 7375.

[19] T. Bollhorst, S. Shahabi, K. Worz, C. Petters, R. Dringen, M. Maas, K. Rezwan, *Angew. Chem.* **2015**, 127, 120.

[20] S. Li, B.A. Moosa, J.G. Croissant, N.M. Khashab, *Angew. Chem.* **2015**, 127, 6908.

[21] H. Jiang, L. Hong, Y. Li, T. Ngai, *Angew. Chem. Int. Ed.* **2018**, 57, 11662.

[22] O.J. Cayre, J. Hitchcock, M.S. Manga, S. Fincham, A. Simoes, R.A. Williams, S. Biggs, *Soft Matter* **2012**, 8, 4717.

[23] S. Zhou, J. Fan, S.S. Datta, M. Guo, X. Guo, D.A. Weitz, *Adv. Funct. Mater.* **2013**, 23, 5925.

[24] Q. Sun, Y. Du, E.A.H. Hall, D. Luo, G.B. Sukhorukov, A.F. Routh, *Soft Matter* **2018**, 14,

2594.
[25] S.U. Pickering, *J. Chem. Soc. Trans.* **1907**, 91, 2001.
[26] J. Wu, G.H. Ma, *Small* **2016**, 12, 4633.
[27] B.P. Binks, Curr. Opin. Colloid Interface Sci. **2002**, 7, 21.
[28] P.H.R. Keen, N.K.H. Slater, A.F. Routh, *Langmuir* **2011**, 28, 1169.
[29] P.H.R. Keen, N.K.H. Slater, A.F. Routh, *Langmuir* **2012**, 28, 16007.
[30] P.H.R. Keen, N.K.H. Slater, A.F. Routh, *Langmuir* **2014**, 30, 1939.
[31] Q. Sun, H. Gao, G.B Sukhorukov, A.F. Routh, *ACS Appl. Mater. Inter.* **2017**, 9, 32599.
[32] A.M.B. Rodriguez, B.P. Binks, *Curr. Opin. Colloid Interface Sci.* **2019**, 44, 107.
[33] K. V. Palamarchuk, T. V. Bukreeva, I. V. Kalashnikova, V. N. Zelenkov, V. V. Potapov, *Colloid journal* **2021**, 83, 228.
[34] J. Li, H.D.H. Stover, Langmuir **2010**, 26, 15554.
[35] F. Yang, S. Ma, W. Zong, N. Luo, M. Lv, Y. Hu, L. Zhou, X. Han, *RSC Adv.* **2015**, 5, 51271.
[36] J.Y. Leong, B.T. Tey, C.P. Tan, E.S. Chan, *ACS Appl. Mater. Interfaces* **2015**, 7, 16169.
[37] P.Y. Tan, T.B. Tan, H.W. Chang, W.W. Mwangi, B.T. Tey, E.S. Chan, O.M. Lai, Y. Liu, Y. Wang, C.P. Tan, *J. Sci. Food Agric.* **2021**, https://doi.org/10.1002/jsfa.11249.
[38] K.L. Thompson, S.P. Armes, J.R. Howse, S. Ebbens, I. Ahmad, J.H. Zaidi, D.W. York, J.A. Burdis, *Macromolecules* **2010**, 43, 10466.
[39] M. Williams, S.P. Armes, D.W. York, *Langmuir* **2012**, 28, 1142.
[40] A. Walsh, K.L. Thompson, S.P. Armes, D.W. York, *Langmuir* **2010**, 26, 18039.
[41] H. Yi, Y. Deng, C. Wang, *Compos. Sci Technol.* **2016**, 133, 51.
[42] Y. Zhao, Y. Li, D.E. Demco, X. Zhu, M. Moller, *Langmuir* **2014**, 30, 4253.
[43] X. Wang, W. Zhou, J. Cao, W. Liu, S. Zhu, *J. Colloid Interface Sci.* **2012**, 372, 24.
[44] K. Stark, J.P. Hitchcock, A. Fiaz, A.L. White, E.A. Baxter, S. Biggs, J.R. McLaughan, S. Freear, O.J. Cayre, *ACS Appl. Mater. Interfaces* **2019**, 11, 12272.
[45] D. Lee, D.A. Weitz, *Small* **2009**, 5, 1932.
[46] D.F.F. Brossault, A.F. Routh, *J. Colloid Interface Sci.* **2020**, 562, 381.
[47] D.F.F. Brossault, T.M. McCoy, A.F. Routh, *J. Colloid Interface Sci.* **2021**, 584, 779.
[48] Y. Ma, J. Yao, *J. Photochem. Photobiol. A* **1998**, 116, 167.
[49] T. Watanabe, T. Takizama, K. Honda, *J. Phys. Chem.* **1977**, 81, 1845.
[50] C. Guo, J. Xu, Y. He, Y. Zhang, Y. Wang, *Appl. Surf. Sci.* **2011**, 257, 3798.